Electronic and optical properties of Cu$_2$XSnS$_4$ (X = Be, Mg, Ca, Mn, Fe, and Ni) and the impact of native defect pairs

Rongzhen Chen, and Clas Persson

Articles you may be interested in

Hierarchical structures of magnetic nanoparticles for controlling magnetic interactions on three different length scales
Journal of Applied Physics **121**, 224303 (2017); 10.1063/1.4983849

Noncollinear antiferromagnetic Haldane magnon insulator
Journal of Applied Physics **121**, 223904 (2017); 10.1063/1.4985615

Electronic and optical properties of Cu$_2$ZnSnS$_4$ and Cu$_2$ZnSnSe$_4$
Journal of Applied Physics **107**, 053710 (2010); 10.1063/1.3318468

Optical properties of bimodally distributed InAs quantum dots grown on digital AlAs$_{0.56}$Sb$_{0.44}$ matrix for use in intermediate band solar cells
Journal of Applied Physics **121**, 214304 (2017); 10.1063/1.4984832

Determining interface properties limiting open-circuit voltage in heterojunction solar cells
Journal of Applied Physics **121**, 185301 (2017); 10.1063/1.4982752

Band offsets of Ag$_2$ZnSnSe$_4$/CdS heterojunction: An experimental and first-principles study
Journal of Applied Physics **121**, 215305 (2017); 10.1063/1.4984315

Electronic and optical properties of Cu$_2$*X*SnS$_4$ (*X* = Be, Mg, Ca, Mn, Fe, and Ni) and the impact of native defect pairs

Rongzhen Chen[1,2,a)] and Clas Persson[1,2,3]

[1]*Department of Materials Science and Engineering, KTH Royal Institute of Technology, SE–100 44 Stockholm, Sweden*
[2]*Centre for Materials Science and Nanotechnology, University of Oslo, P.O. Box 1048 Blindern, NO-0316 Oslo, Norway*
[3]*Department of Physics, University of Oslo, P.O. Box 1048 Blindern, NO–0316 Oslo, Norway*

Reducing or controlling cation disorder in Cu$_2$ZnSnS$_4$ is a major challenge, mainly due to low formation energies of the anti-site pair (Cu$_{Zn}^-$ + Zn$_{Cu}^+$) and the compensated Cu vacancy (V$_{Cu}^-$ + Zn$_{Cu}^+$). We study the electronic and optical properties of Cu$_2$*X*SnS$_4$ (C*X*TS, with *X* = Be, Mg, Ca, Mn, Fe, and Ni) and the impact of defect pairs, by employing the first-principles method within the density functional theory. The calculations indicate that these compounds can be grown in either the kesterite or stannite tetragonal phase, except Cu$_2$CaSnS$_4$ which seems to be unstable also in its trigonal phase. In the tetragonal phase, all six compounds have rather similar electronic band structures, suitable band-gap energies E_g for photovoltaic applications, as well as good absorption coefficients $\alpha(\omega)$. However, the formation of the defect pairs (Cu$_X$ + X_{Cu}) and (V$_{Cu}$ + X_{Cu}) is an issue for these compounds, especially considering the anti-site pair which has formation energy in the order of ∼0.3 eV. The (Cu$_X$ + X_{Cu}) pair narrows the energy gap by typically $\Delta E_g \approx$ 0.1–0.3 eV, but for Cu$_2$NiSnS$_4$, the complex yields localized in-gap states. Due to the low formation energy of (Cu$_X$ + X_{Cu}), we conclude that it is difficult to avoid disordering from the high concentration of anti-site pairs. The defect concentration in Cu$_2$BeSnS$_4$ is however expected to be significantly lower (as much as ∼10^4 times at typical device operating temperature) compared to the other compounds, which is partly explained by larger relaxation effects in Cu$_2$BeSnS$_4$ as the two anti-site atoms have different sizes. The disadvantage is that the stronger relaxation has a stronger impact on the band-gap narrowing. Therefore, instead of trying to reduce the anti-site pairs, we suggest that one shall try to compensate (Cu$_X$ + X_{Cu}) with (V$_{Cu}$ + X_{Cu}) or other defects in order to stabilize the gap energy. *Published by AIP Publishing.* [http://dx.doi.org/10.1063/1.4984115]

I. INTRODUCTION

Chalcopyrite materials are an attractive group of materials for thin film photovoltaics (PV). Cu$_2$ZnSn(S,Se)$_4$ (CZTSSe) is considered as a promising absorber material, and the best research cell efficiency today is ∼12.6% achieved in the lab condition.[1] There are extensive investigations and developments of CZTSSe world-wide, and many of these studies focus on understanding the defects in the material.[2–9] Researchers also started to explore similar compounds but substituting Zn by transition metal atoms, such as Mn, Fe, Co, and Ni. For instance, the fundamental band-gap energy E_g of Cu$_2$MnSnS$_4$ is experimentally estimated to be between 1.18 and 1.63 eV depending on the heat treatment,[10] and a solar cell based on Cu$_2$MnSnS$_4$ has an efficiency of 0.49%. The band-gap energies of synthesized Cu$_2$FeSnS$_4$ nanocrystals and Cu$_2$CoSnS$_4$ and Cu$_2$NiSnS$_4$ nanoparticles are ∼1.33 or ∼1.5 eV,[11,12] ∼1.40[13] and ∼1.40 eV,[14,15] respectively. Moreover, kesterite Cu$_2$MgSnS$_4$ nanoparticles without a secondary phase have been synthesized using a hot-injection method.[16] From first-principles calculations with the generalized gradient approximation (GGA), Wang *et al.*[17] have found that kesterite

Cu$_2$CdSnS$_4$ and Cu$_2$HgSnS$_4$ are thermodynamically stable, but kesterite Cu$_2$MgSnS$_4$ and especially kesterite Cu$_2$CaSnS$_4$ are not stable. Complementarily, Zhong *et al.*[18] found, using a hybrid functional, that stannite Cu$_2$MgSnS$_4$ (and Cu$_2$MgSnSe$_4$) is thermodynamically stable, but, similar to Wang *et al.*, that kesterite and stannite phases of Cu$_2$CaSnS$_4$ (and Cu$_2$CaSnSe$_4$) are unstable with respect to competing compounds.

Some of the above-mentioned compounds can be alternative candidates as thin film PV materials; however, better knowledge of the synthesis processes as well as a deeper understanding of the impact of native defects is needed. That is, in Cu$_2$ZnSnS$_4$ (CZTS), copper vacancy V$_{Cu}^-$ is an important shallow acceptor, and the anti-site defects involve shallow donors Zn$_{Cu}^+$ and shallow acceptors Cu$_{Zn}^-$.[5,19] It is known that Cu-Zn disorder induces band-gap energy fluctuations in the material.[4] Therefore, it is important to investigate how to reduce the concentration of the anti-site pair (ASP) in CZTSSe. Yuan *et al.*[20] suggested that Zn shall be substituted by the large-size atom Cd and alternative Cu substituted by Ag, to suppress the formation of anti-site defects. They found that while Cd$_{Cu}^+$ in Cu$_2$CdSnS$_4$ had as low formation energy as Zn$_{Cu}^+$ in CZTS, the corresponding anti-site Zn$_{Ag}^+$ in Ag$_2$ZnSnS$_4$ had significantly much higher formation energy. Therefore, further investigations of C*X*TSSe (i.e., where Zn is replaced by the element *X*) are expected to

a)Author to whom correspondence should be addressed: Rongzhen.Chen@mse.kth.se

reveal a fundamental understanding of the defect physics in these quaternary chalcopyrites.

In this work, the electronic and optical properties as well as the formation of native ASP defects ($Cu_X + X_{Cu}$) and ($V_{Cu} + X_{Cu}$) are theoretically explored for tetragonal Cu_2XSnS_4 (CXTS, with $X =$ Be, Mg, Ca, Mn, Fe, and Ni) within the framework of the density functional theory (DFT). We consider the transition metal atoms Mn, Fe, and Ni to study the magnetic effects, and we include Be to analyze if local relaxation for a small-size atom suppresses the disorder due to ASPs. Mg is interesting as Cu_2MgSnS_4 is experimentally prepared and investigated. Ca is included in order to study trends in the band-gap energies E_g, the optical properties, and the defect formation energies for compounds with group-IIA elements. For the considered quaternary chalcopyrites, there are to our knowledge no earlier defect studies on Cu_2BeSnS_4, Cu_2MnSnS_4, Cu_2FeSnS_4, and Cu_2NiSnS_4 and only a few defect studies on the other compounds.

We find that for tetragonal Cu_2MgSnS_4, Cu_2CaSnS_4, Cu_2FeSnS_4, and Cu_2MnSnS_4, the stannite (ST) phase is more stable (or at least less unstable) compared to the kesterite (KS) phase, while the opposite is true for Cu_2BeSnS_4 and Cu_2NiSnS_4. For Cu_2CaSnS_4, the formation energy of the trigonal phase is lower than that of the ST phase, but even the trigonal phase of Cu_2CaSnS_4 is not stable with respect to chemical decomposing compounds. The absorption coefficients of CXTS are calculated with a dense **k**-mesh,[21] and we find that overall the coefficients are similar to those of CZTS apart from having slightly different onset energies. Remarkably, the absorption coefficient of Cu_2NiSnS_4 is much higher in a broad energy range than those of the other compounds, and this compound has a band-gap energy close to the optimum value ($\sim$1.3 eV) for maximum device efficiency in the Shockley-Queisser (SQ) limit.[22,23] From the defect analysis, however, we find that Cu_2FeSnS_4 and Cu_2NiSnS_4 may not be suitable PV absorber materials as their point defect or ASP forms localized in-gap states. Cu_2MgSnS_4 and Cu_2MnSnS_4 have similar (but somewhat smaller) absorption coefficients and similar ASP formation energies compared to CZTS. From that perspective, substituting Zn by $X =$ Mg or Mn is not expected to improve the PV properties. Cu_2BeSnS_4, on the other hand, has a higher absorption coefficient between $E_g + 0.6$ eV and $E_g + 1.2$ eV than CZTS for its corresponding energy region. Moreover, partly due to stronger relaxation effects, Cu_2BeSnS_4 also has higher defect formation energy of its ASP, implying that the ASP concentration in Cu_2BeSnS_4 is significantly lower than in the other CXTS compounds. The disadvantage of Be is of course handling of the element and its toxicity.

II. COMPUTATIONAL DETAILS

The calculations are performed by means of the plane augmented wave formalism within the DFT as implemented in the VASP program package.[24,25] CXTS typically crystallize in the KS phase (space group S_4^2; no. 82) or in the ST phase (D_{2d}^{11}; no. 121). We determine the ground state phase from the total energy, via a fully relaxed process. For Cu_2MnSnS_4, Cu_2FeSnS_4, and Cu_2NiSnS_4 with magnetic transition metal atoms, we consider the ferromagnetic and

three antiferromagnetic (AFM) configurations (in both the KS and ST phases). For Cu_2CaSnS_4, we compare some results with the trigonal phase (space group C_3^2; no. 144). Cu_2XSnS_4 ($X =$ Be, Mg, and Ca) and CZTS are relaxed using the Perdew-Burke-Ernzerhof[26] GGA exchange-correlation functional revised for solids (PBEsol).[27] Cu_2XSnS_4 ($X =$ Mn, Fe, and Ni) are relaxed with PBEsol with an onsite Coulomb interaction correction[28] of the d-like orbitals for the transition metal atoms (i.e., PBEsol + U) since it has been demonstrated that this correction is crucial to accurately determine the magnetic configuration and lattice parameters for magnetic materials using local potential,[29] which also our test calculation confirms. Here, we choose $U_d(Mn) = 4.0$ eV, $U_d(Fe) = 4.6$ eV, $U_d(Ni) = 5.1$ eV, and $U_d(Cu) = 4$ eV, according to Setyawan et al.[30] With the corrected potential on the d-like orbitals, the d-like energy states are corrected and the band gap is also opened moderately (by $\sim$0.3 eV), which is a normal effect in semiconductors with strong d-like states in the valence bands.[31] The crystalline structures are fully relaxed until the total energy and the residual force on each atom show convergence within 0.1 and 10 meV/Å, respectively. From the relaxed structures, the total energies of the structure (both defect-free and crystals with defects) are determined from the Heyd-Scuseria-Ernzerhof functional with the standard parameters for mixing and screening (i.e., HSE06).[32]

The electronic and optical properties of the defect-free compounds are modeled using 16 atom unit cells. For the defect calculations, we use relatively small unit cells of 64 atoms, which simulate neutral native defects at high concentrations in order to see how disorder changes the band-gap energy. The use of small cells is also justified by the fact that we focus the study on neutral defects, and we do not calculate transition energies. The band structure and density-of-states (DOS) are computed with the HSE06 potential, and we estimate that the error bar of predicted fundamental band-gap energies is 0.1–0.2 eV, which is a typical error bar for the HSE06. The DOS is calculated for the large-cell structures with defects using K $= 2 \times 2 \times 2$ Γ-centered Monkhorst-Pack like **k**-meshes. The optical properties, however, require a much larger **k**-mesh for describing details in the dispersion of the optical transitions,[21] especially for photon energies near the band-gap energy. Therefore, the absorption coefficients $\alpha(\omega)$ of Cu_2XSnS_4 are modeled with K $= 16 \times 24 \times 24$ Γ-centered **k**-meshes, which implies 4612 **k**-points in the irreducible Brillouin zone (IBZ). The absorption coefficients are determined directly from the complex dielectric function, using the modified tetrahedron integration method with a 0.01 eV smearing in the Kramers-Kronig transformation relation. For computational reasons, we use PBEsol for $X =$ Be, Mg, and Ca and PBEsol + U for $X =$ Mn, Fe, and Ni. Overall, the results obtained by using these potentials and a smaller **k**-mesh agree fairly well with the corresponding spectra obtained from HSE06 calculations.

III. RESULTS

A. Crystalline phases, electronic structures, and optical properties

The CXTS compounds are analyzed for the tetragonal KS or ST structures. For Cu_2MnSnS_4, Cu_2FeSnS_4, and

Cu_2NiSnS_4, we consider four magnetic phases (one ferromagnetic and three antiferromagnetic configurations), and the most stable magnetic configuration is the antiferromagnetic phase described by the yellow arrows in Fig. 1. The most stable configurations for ST and KS are henceforth denoted as ST-AFM and KS-AFM. From the total energy E_{tot}, we find that the most stable structures are KS, ST, ST, ST-AFM, ST-AFM, and KS-AFM for $CXTS$ with $X =$ Be, Mg, Ca, Mn, Fe, and Ni, respectively. CZTS is known to have KS as its most stable phase. The total energy differences between the KS and ST phases are 198, 37, 479, and 50 meV/cell (16 atom cell) for Cu_2BeSnS_4, Cu_2MgSnS_4, Cu_2CaSnS_4, and Cu_2ZnSnS_4, respectively. Specifically for Cu_2MgSnS_4 (and also for Cu_2ZnSnS_4), the presence of secondary phases in the materials is most likely possible. For Cu_2MnSnS_4, the total energy differences between the most stable phase (ST-AFM) and other phases are between 4 and 59 meV/cell. The larger value is from the kesterite ferromagnetic phase, whereas the

maximal absolute energy differences between the four magnetic configurations are only 24 and 25 meV/cell for ST and KS, respectively. This may indicate that the paramagnetic phase can exist depending on growth conditions and temperature for Cu_2MnSnS_4. For Cu_2FeSnS_4, the total energy differences between stable (ST-AFM) and other phases are between 16 and 30 meV per cell; here, the larger value is from the kesterite antiferromagnetic phase. Similarly, for Cu_2NiSnS_4, the total energy differences between stable (KS-AFM) and other phases are between 95 and 1700 meV/cell; here, the larger value is from the stannite antiferromagnetic phase. The large energy difference demonstrates that the compound has a strong magnetic phase that governs its crystalline structure.

The energy with respect to the formation energy of chemical decomposition, i.e., $Cu_2XSnS_4 \rightarrow [2(CuS) + XS + SnS]$, $[Cu_2S + XS + SnS_2]$, or $[Cu_2SnS_3 + XS]$, indicates possibility for being stable as a compound. Here, Cu_2MnSnS_4 and Cu_2FeSnS_4 are clearly stable chalcopyrites. Cu_2NiSnS_4 is also a theoretically stable compound from this analysis although the energy to decompose is smaller, and this is supported by the fact that at least nanoparticles have been synthesized.[14,15] The tetragonal compounds containing the group-IIA elements are known to be less stable (or unstable).[17,18] We find a trend that the light Be or Mg atom forms a $CXTS$ crystal with lower formation energy compared to its decomposing compounds, while heavier Ca elements make the crystal unstable. Thereby, Cu_2BeSnS_4 and Cu_2MgSnS_4 have stable KS and ST phases, respectively. Although the trigonal phase is preferable for Cu_2CaSnS_4, this phase is also unstable with respect to decomposition. However, the Cu_2BaSnS_4 compound, with an even heavier group-IIA element, has a stable trigonal phase,[33] which also our test calculations demonstrate (not presented in this work). For Cu_2MgSnS_4 and Cu_2NiSnS_4, the choice of exchange-correlation potential can make deviations. We use HSE06; however, with the PBEsol(+U) potential, the formation energies of the compounds are higher than those of chemical decompositions $([Cu_2SnS_3 + MgS/NiS])$; thereby, they can be unstable. This probably explains the somewhat disagreeing results in the earlier studies.[17,18]

In Table I, we present the crystal parameters for the most stable tetragonal structure of the $CXTS$ compounds, and only these configurations are henceforth considered in this study (unless specifically stated). As expected, the bond length of the compounds follows the sum of covalent radii of the atoms. For example, the bond length $\delta(Cu–S)$ is between 2.28 and 2.32 Å in our results, and the covalent radii of Cu and S are ~1.32 and ~1.05 Å. This also holds for $\delta(X–S)$: for example, the calculated bond length $\delta(Mg–S)$ is ~2.45 Å, and the covalent radius of Mg is ~1.41 Å. The lattice ratio c/a is less than 2 for $CXTS$, which indicates a stronger relaxation with respect to the ideal zinc-blende-like atomic positions. The stronger relaxation is also obvious from the anion positions (see Table I). Experimentally, the lattice constants for ST Cu_2MnSnS_4 at temperature $T = 15.2$ K are $a = 5.514$ Å and $c/a = 1.957$,[34] and our results ($a = 5.473$ Å and $c/a = 1.960$) are in good agreement with these.

The electronic structures and the atomic and angular-momentum dependent DOS (PDOS) of $CXTS$ and CZTS are
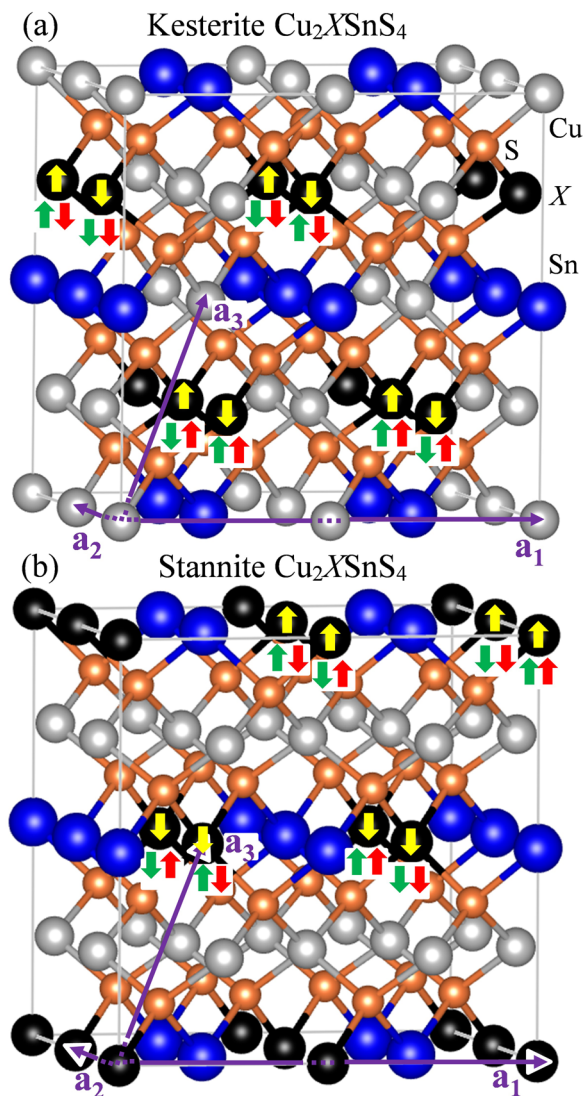

FIG. 1. Crystalline structures of (a) kesterite and (b) stannite Cu_2XSnS_4, where the magnetic configurations are indicated by the arrows. The yellow arrows on the X-atom site show the most stable antiferromagnetic phase for $X =$ Mn, Fe, and Ni, while green and red arrows indicate two other antiferromagnetic configurations, respectively, both with higher formation energy. Also, the ferromagnetic phase has higher formation energy.

TABLE I. The crystalline lattice parameters a and c/a and the bond lengths δ(cation–S) are presented for the most stable tetragonal phase of Cu_2XSnS_4 (X = Be, Mg, Ca, Mn, Fe, and Ni) and Cu_2ZnSnS_4. The available experimental lattice parameters (Refs. 34–37) are presented in parentheses.

	KS Cu_2BeSnS_4	ST Cu_2MgSnS_4	ST Cu_2CaSnS_4	ST-AFM Cu_2MnSnS_4	ST-AFM Cu_2FeSnS_4	KS-AFM Cu_2NiSnS_4	KS Cu_2ZnSnS_4
a (Å)	5.263	5.489	5.809	5.473 (5.514[a])	5.432 (5.450[b])	5.464	5.372 (5.428[c])
c/a	1.971	1.955	1.765	1.960 (1.957[a])	1.952 (1.968[b])	1.903	2.001 (2.002[c])
S position							
x	0.750	0.749	0.729	0.750	0.756	0.755	0.768 (0.756[d])
y	0.778	0.749	0.730	0.750	0.756	0.768	0.759 (0.757[d])
z	0.862	0.862	0.852	0.863	0.866	0.867	0.870 (0.872[d])
δ(Cu–S) (Å)	2.275	2.283	2.316	2.286	2.277	2.296	2.275
δ(X–S) (Å)	2.111	2.449	2.694	2.436	2.350	2.280	2.329
δ(Sn–S) (Å)	2.430	2.436	2.422	2.430	2.427	2.450	2.443

[a]Fries *et al.*[34]
[b]Bonazzi *et al.*[35]
[c]Schorr *et al.*[36]
[d]Hall *et al.*[37]

presented in Fig. 2 (Cu_2FeSnS_4 is fairly similar to Cu_2MnSnS_4, and the results are therefore presented in the supplementary material). The band-gap energies are $E_g = 1.76$, 1.48, 1.84, 1.40, 1.71, 1.26, and 1.29 eV for CXTS (with X = Be, Mg, Ca, Mn, Fe, and Ni) and CZTS, respectively, obtained from the HSE06 calculations. These gap energies are in fairly good agreement with available experimental results for Cu_2MgSnS_4 ($E_g = 1.63$ eV), Cu_2MnSnS_4 (1.18–1.63 eV), Cu_2FeSnS_4 (1.33 or 1.5 eV), Cu_2NiSnS_4 (1.40 eV), and CZTS (1.45 eV).[10–12,14,15,38]

The electronic structures and PDOS of CXTS are qualitatively similar to those of CZTS (Fig. 2). Cu d-like states hybridize with S p-like states in a wide energy range in the valence band (VB) below the VB maximum (VBM). For the conduction band (CB) states, the DOS is comparable for CXTS (except Cu_2NiSnS_4) and CZTS, at least from the conduction band minimum (CBM) to some ~3 eV up in energy. Here, it is mainly hybridization between the Sn s-like and S p-like states. It is also noticeable that Ca and Mn d-like states hybridize with Sn p-like states in the energy range above 3 eV.
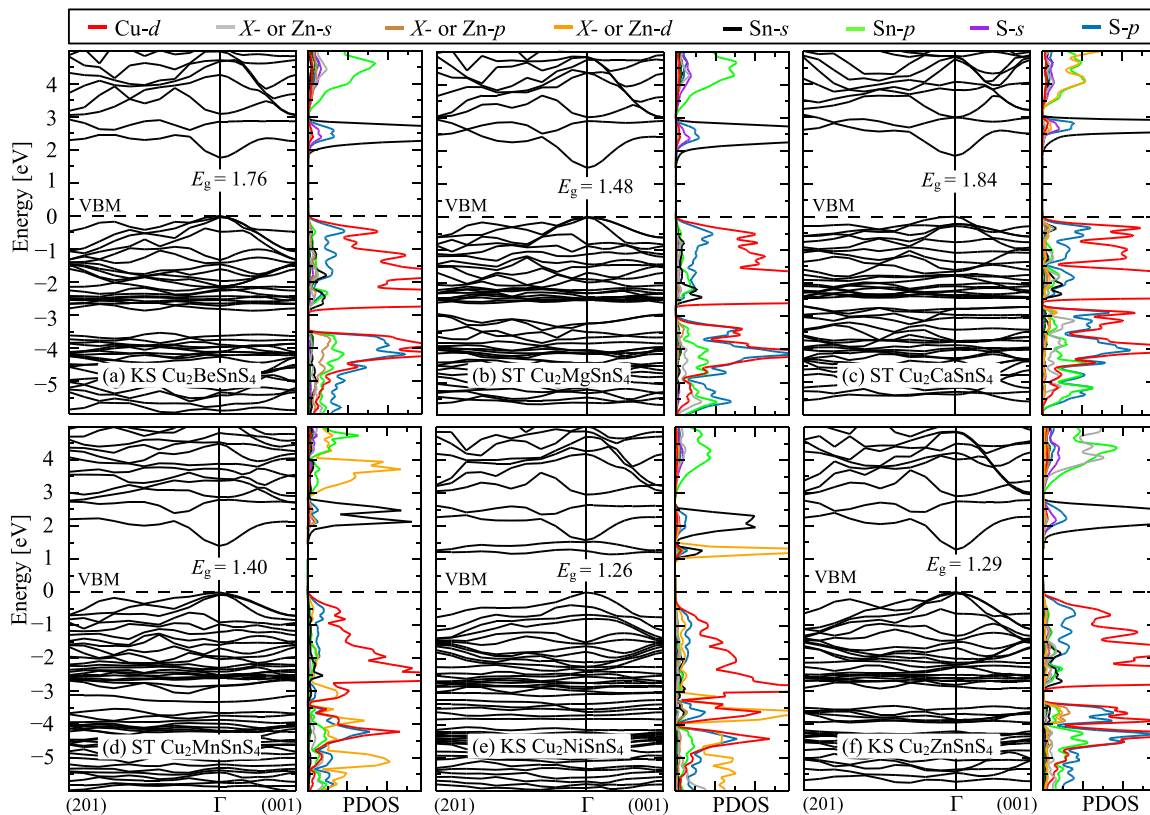

FIG. 2. The electronic band structure and the atom and angular-momentum resolved DOS (PDOS) for the non-magnetic (a) kesterite Cu_2BeSnS_4, (b) stannite Cu_2MgSnS_4, and (c) stannite Cu_2CaSnS_4. The corresponding band structure and PDOS for the magnetic (d) stannite Cu_2MnSnS_4 and (e) kesterite Cu_2NiSnS_4; the two spin components are not distinguishable. For comparison, the band structure and DOS of (f) kesterite Cu_2ZnSnS_4 are also presented. For better visibility, the PDOS is scaled with $1/(2\ell + 1)$, where ℓ is the angular-momentum quantum number, and presented with a 50 meV Lorentzian broadening.

Cu_2NiSnS_4 is quite different from the others in the aspects of the electronic band structure and PDOS. For instance, in Cu_2NiSnS_4, it is mainly the Ni d-like states that hybridize with Sn s-like states between CBM and CBM + 1 eV. As a consequence of this, Cu_2NiSnS_4 has an indirect band gap, in contrast to the other considered compound. However, the indirect band-gap energy of Cu_2NiSnS_4 is energetically close to the gap energy at the Γ-point; the difference is only ~10 meV. This is a consequence of that the lowest CB of Cu_2NiSnS_4 is very flat, which then in turn can imply advantageously strong photon absorption. However, the disadvantage can be a large effective electron mass.

In Fig. 3, the calculated absorption coefficients $\alpha(\omega)$ of CXTS are presented. A clear onset of absorption occurs near the band-gap energy for all compounds, indicating good dipole-allowed transition probability. Also, all compounds have absorption coefficients similar to CZTS. To better compare $\alpha(\omega)$ for compounds with different band-gap energies, the absorption coefficients in Fig. 3(b) are presented on the energy scale ($\hbar\omega - E_g$). One notices that most compounds have a pronounced absorption peak at ~1.3 eV, and this peak is at ~1.0 eV for Cu_2BeSnS_4 and ~0.8 eV for Cu_2NiSnS_4.

It is therefore obvious that Cu_2NiSnS_4 has a much better absorption in the energy region E_g and $E_g + 1.0$ eV compared to CZTS, and Cu_2NiSnS_4 has a good absorption coefficient in a broad energy range due to the very flat Ni d-like CBs (cf. Fig. 2). Cu_2BeSnS_4 has a higher absorption coefficient than CZTS between $E_g + 0.6$ eV and $E_g + 1.2$ eV, while Cu_2MgSnS_4, Cu_2MnSnS_4, and Cu_2FeSnS_4 have similar absorption to CZTS from E_g to about $E_g + 1$ eV.

It is worth noticing that, in the calculations for absorption coefficients, a rather dense **k**-mesh is utilized in the calculations in order to generate a more detailed shape of the absorption spectra near E_g.[21] Furthermore, based on earlier studies,[8,39] we expect that the corresponding Se-based compounds (i.e., CXTSe) shall have similar electronic and optical properties to their S-based counterparts but that their corresponding band-gap energies are ~0.5 eV smaller due to the heavier anion atom.

B. Native defects

To analyze the impact of native defect pairs that contain Cu vacancies and/or anti-sites, we model and perform calculations of defects in supercells with 64 atoms. One issue regarding the CZTS material is that Cu–Zn disorder introduces a band-gap fluctuation.[4] Therefore, it is of interest not only to calculate how especially ASPs affect the band-gap energies with ASPs but also to calculate the defect formation energy of the compounds in order to suggest if it is possible to reduce the disorder by doping, alloying, or in some other ways. The formation energy of the defect is defined by $\Delta H(D) = E_{tot}(CXTS:D) - E_{tot}(CXTS) + \Sigma_\alpha n_\alpha \cdot \mu_\alpha$. Here, $E_{tot}(CXTS:D)$ and $E_{tot}(CXTS)$ are the total energies for CXTS with and without defect D, respectively, and $n_\alpha = -1$ (+1) when one atom α is added (removed). The chemical potential is expressed as $\mu_\alpha = \mu_{\alpha,sol} + \Delta\mu_\alpha$, where $\mu_{\alpha,sol}$ is the total energy per atom of the solid compound for element α.[40] $\Delta\mu_\alpha$ can vary depending on the external condition, and for simplicity, we set $\Delta\mu_\alpha = 0$ (α-rich conditions) since the focus is on ASPs in this study with $n_\alpha = 0$. The binding energy $E_b(D)$ for the complex $D = (D_1 + D_2)$ containing the two defects D_1 and D_2 is calculated as $E_b(D) = [E_{tot}(CXTS:D) + E_{tot}(CXTS)] - [E_{tot}(CXTS: D_1) + E_{tot}(CXTS:D_2)]$.

The calculated $\Delta H(D)$ and $E_b(D)$ of the native, neutral complexes ($V_{Cu} + X_{Cu}$) and ($Cu_X + X_{Cu}$) in CXTS are presented in Table II; native single defects of CZTS are also shown for comparison. In Fig. 4, we compare the total DOS of CXTS with V_{Cu}, Cu_X, X_{Cu}, and ($Cu_X + X_{Cu}$) defects with the corresponding DOS of the defect-free compound. First, and without considering the Cu_2FeSnS_4 and Cu_2NiSnS_4 compounds, the single defects V_{Cu} and X_{Cu} overall have a moderate effect on the electronic structure. For all the compounds, the V_{Cu}^- and Cu_X^- defects induce rather shallow acceptor states at the VBM, and thus, the Fermi level E_F is below VBM. V_{Cu}^- is a very delocalized acceptor that has a minor effect on the VB states and acts almost as a hole carrier doping. However, the smaller Cu-d–S-p repulsion when the copper-poor V_{Cu}^- defect is present implies that the band-gap energy is increased (typically by $\Delta E_g \approx 0.1$ eV for a defect concentration of 1.5%), except for ST Cu_2CaSnS_4. Here, the change in gap
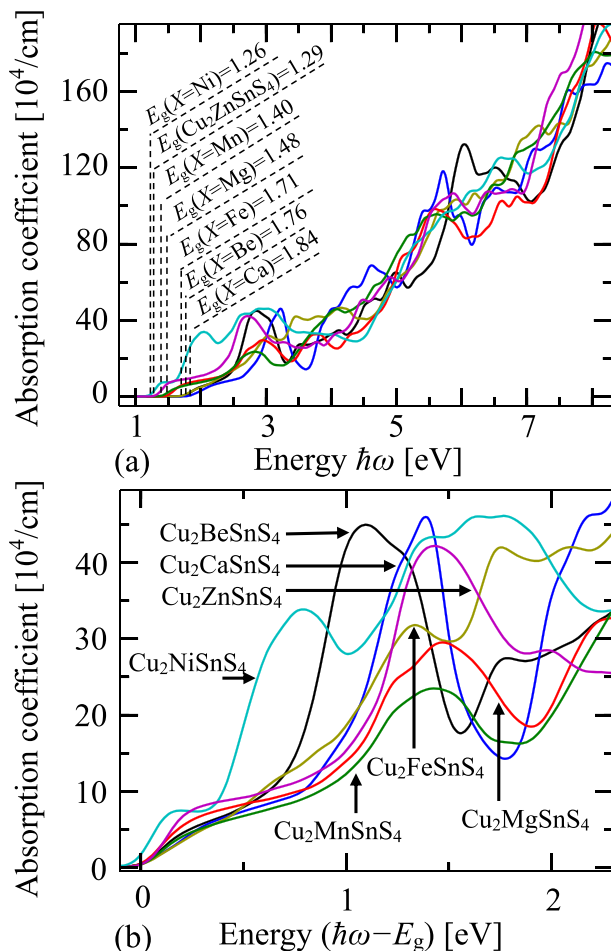

FIG. 3. Absorption coefficients $\alpha(\omega)$ of CXTS and Cu_2ZnSnS_4 from the PBEsol (+U) calculations with band-gap energies E_g adjusted to the HSE06 results: (a) with respect to the photon energy $\hbar\omega$ and (b) a close-up near the absorption onset, where the energy scale is ($\hbar\omega - E_g$), to better compare the six compounds. The spectra are presented with an additional 50 meV Lorentzian broadening to the spectrum.

TABLE II. Defect formation energy $\Delta H(D)$ for $\Delta\mu_\alpha = 0$, binding energy $E_b(D)$ of defect pairs, and the induced shift $\Delta E_g(D)$ of the gap energy for native defects in tetragonal CXTS; all units are in eV. Total magnetic moment M_t units in μ_B are given for Cu$_2$MnSnS$_4$ and Cu$_2$NiSnS$_4$ including the defects, where the local magnetic moment is $\sim$4.4μ_B for Mn (4.28μ_B in Ref. 34), $\sim$3.5μ_B for Fe, and $\sim$1.5μ_B for Ni.

Compound	Phase		V_{Cu}	V_X	X_{Cu}	Cu_X	$(V_{Cu}+X_{Cu})$	(Cu_X+X_{Cu})
Cu$_2$BeSnS$_4$	KS	ΔH	1.50	4.14	0.19	2.33	−0.28	0.58
		E_b					−1.97	−1.94
		ΔE_g	0.00	−0.12	−0.22	−0.26	0.07	−0.30
Cu$_2$MgSnS$_4$	ST	ΔH	1.61	4.85	−0.52	2.83	−1.07	0.34
		E_b					−2.17	−1.97
		ΔE_g	0.07	−0.07	−0.10	−0.22	0.10	−0.18
Cu$_2$CaSnS$_4$	ST	ΔH	1.14	5.92	−1.86	3.86	−2.68	0.13
		E_b					−1.95	−1.87
		ΔE_g	−0.07	−0.14	−0.22	−0.34	0.02	−0.29
Cu$_2$MnSnS$_4$	ST-AFM	ΔH	1.60	4.37	−0.21	2.35	−0.54	0.33
		E_b					−1.93	−1.81
		ΔE_g	0.05	−0.35	−0.21	−0.37	0.06	−0.19
		M_t	0.1	3.0	4.6	4.0	5.0	0.0
Cu$_2$FeSnS$_4$	ST-AFM	ΔH	1.64	5.94	−1.67	3.81	−2.01	0.35
		E_b					−1.98	−1.80
		ΔE_g	−0.02	−0.83	−1.08	−0.26	0.01	−0.17
		M_t	0.3	2.0	2.8	2.8	3.7	0
Cu$_2$NiSnS$_4$	KS-AFM	ΔH	1.57	3.09	−0.22	1.08	0.60	0.36
		E_b					−0.75	−0.49
		ΔE_g	−0.07	−0.18	0.00	−0.22	−0.15	−0.53
		M_t	0.1	2.0	1.0	2.8	2.0	0.0
Cu$_2$ZnSnS$_4$	KS	ΔH	1.42	3.54	0.45	1.64	−0.09	0.30
		E_b					−1.96	−1.79
		ΔE_g	0.06	−0.03	−0.13	−0.12	0.08	−0.13

energy refers to changes in the host-like VBM and/or CBM, while the free hole (electron) concentration from the acceptors (donors) implies a larger optical band gap (about 0.2–0.3 eV for a defect concentration of 1.5%). Furthermore, the copper-rich Cu$_X^-$ acceptor forms somewhat more localized acceptor states, and these acceptor states shift the VBM energetically upwards. Thereby, the gap energy is decreased ($\Delta E_g \approx$ –0.1 to –0.4 eV), in contrast to V$_{Cu}^-$. The X_{Cu}^+ defect induces shallow donor states with the Fermi level in the CB, and the donor shifts the CBM energetically downwards. Thus, similar to the Cu$_X^-$ acceptor, the X_{Cu}^+ donor narrows the gap ($\Delta E_g \approx 0$ to –0.2 eV) despite that it involves less Cu-d–S-p repulsion. The calculated change in the band-gap energy of CZTS is similar to what has been reported previously,[4,41] where the band-gap energies are reduced by $\sim$0.1 eV for Zn$_{Cu}^0$ and increased by $\sim$0.1 eV for V$_{Cu}^-$.

From the total energies (Table II), we find that CXTS has similar formation energy of V$_{Cu}$ to CZTS in the Cu-rich limit. This indicates that it is possible to form non-stoichiometric compounds for these CXTS. Moreover, the formation energies of the other single point defects are relatively small (see also Ref. 5), and they can thus easily compensate each other (or other charged defect). Thus, the oppositely charged point defects V$_{Cu}^-$ (or Cu$_X^-$) and X_{Cu}^+ can be compensated to form neutral complex Cu-poor (V$_{Cu}^-$+X_{Cu}^+)^0 or ASP (Cu$_X^-$+X_{Cu}^+)^0. The calculated binding energies $E_b(D)$ verify that compensated Cu vacancy defects and/or APS are favorable. We find

that the binding energies of (V$_{Cu}^-$+X_{Cu}^+) and ASP (Cu$_X^-$+X_{Cu}^+) are as large as $|E_b(D)| > 1$ eV. This is not so surprising considering that the two constituents are one single acceptor and one single donor, and the energy gain when compensating the donor (or acceptor) is roughly 1 eV when the donor electron (or the acceptor hole) is captured across the band gap with $E_g \approx 1.5$ eV. Hence, (Cu$_X^-$+X_{Cu}^+) and (V$_{Cu}^-$+X_{Cu}^+) form neutral complexes, and one can therefore easily have high concentrations of them.

The formation energy of the ASP does not depend on the external chemical potential of the elements, and we find that $\Delta H(D)$ of (Cu$_X^-$+X_{Cu}^+) is low. Here, Cu$_2$MgSnS$_4$, Cu$_2$MnSnS$_4$, Cu$_2$FeSnS$_4$, Cu$_2$NiSnS$_4$, and CZTS have similar defect formation energies ($\sim$0.3 eV). However, Cu$_2$BeSnS$_4$ has a relatively high defect formation energy (0.58 eV) for its ASP complex. One reason for the larger $\Delta H(D)$ is that the atom size of Be is much smaller than the sizes of both Cu and Sn, and the relaxation effect is therefore stronger. For instance, the energy difference of $\Delta H(D)$ between structures with unrelaxed and relaxed (Cu$_X^-$+X_{Cu}^+) defects is 0.60 eV in Cu$_2$MgSnS$_4$, while 0.96 eV in Cu$_2$BeSnS$_4$. This extra relaxation effect implies that the formation energy of APS is $\sim$0.3 eV larger in Cu$_2$BeSnS$_4$ than in similar compounds. This 0.3 eV energy difference may seem to be small, but the defect concentration depends exponentially on defect formation energy: $[N(D)] = N_s g_q \exp[-\Delta H(D)/(k_B T)]$, where N_s is the possible defect sites and g_q is the degeneracy factor. $k_B T$
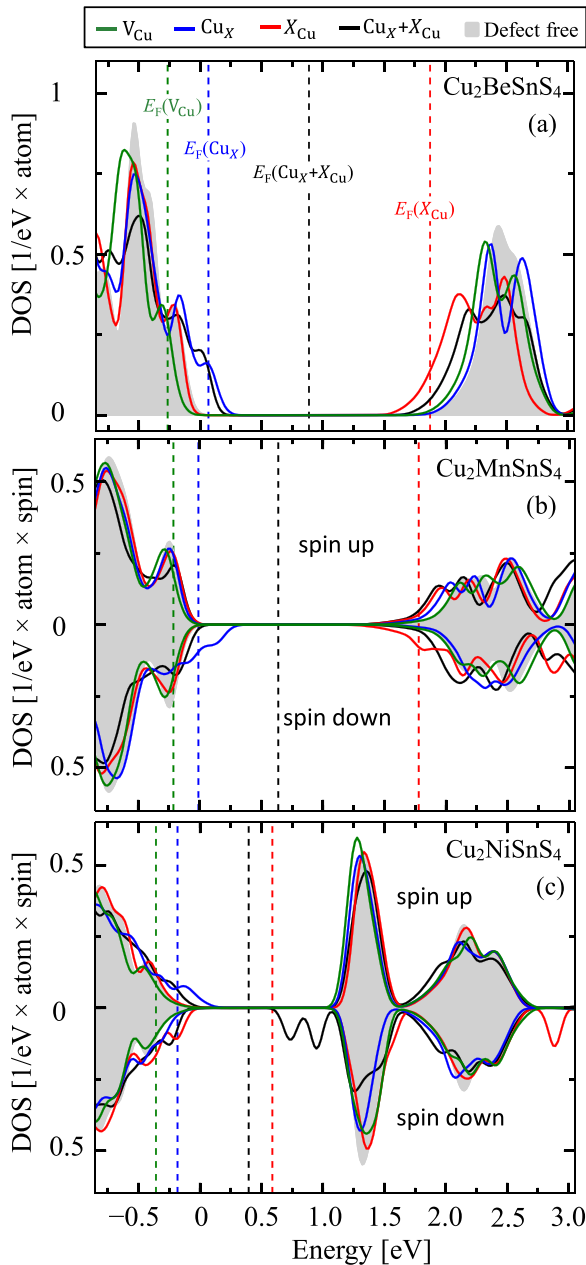
FIG. 4. The total DOS of compounds with the defects V_{Cu} (green lines), Cu_X (blue lines), X_{Cu} (red lines), and ($Cu_X + X_{Cu}$) (black lines), and for comparison, the corresponding DOS for the defect free case (grey area): (a) Cu_2BeSnS_4, (b) Cu_2MnSnS_4, and (c) Cu_2NiSnS_4. The non-magnetic Cu_2MgSnS_4, Cu_2CaSnS_4, and Cu_2ZnSnS_4 compounds with defects have qualitatively similar DOS to Cu_2BeSnS_4, and Cu_2FeSnS_4 has similar DOS to Cu_2MnSnS_4 apart from having localized in-gap states for Fe_{Cu}; see supplementary material. The energy refers to VBM of the defect free compound, and the DOS alignment for defects is estimated simply by aligning the semi-core S s-like states. The Fermi levels are indicated with dashed lines, and the DOS are presented with a 50 meV Lorentzian broadening. Spin up and spin down DOS are shown for Cu_2MnSnS_4 and Cu_2NiSnS_4.

is ∼0.03 eV at room temperature, which is only ∼1/10 of the considered defect formation energy, and small variations in $\Delta H(D)$ have therefore a large effect on [$N(D)$]. With N_s and g_q fixed, we estimate that the concentration [($Cu_X^- + X_{Cu}^+$)] is as much as ∼10^4 times lower in Cu_2BeSnS_4 than in Cu_2MgSnS_4, Cu_2MnSnS_4, Cu_2FeSnS_4, Cu_2NiSnS_4, and CZTS. Since ST Cu_2CaSnS_4 has very low ASP formation

energy (0.13 eV), the compound is expected to be disordered or actually chemically decomposed. Its trigonal phase has much higher formation energy of its ASP (1.40 eV), and this phase will have a negligible ASP concentration (see Table SI in the supplementary material), but the compound is unfortunately not stable as already discussed.

We also confirm earlier published results[19] that the ASP in Cu_2CdSnS_4 is as easy to be formed as in CZTS despite the larger Cd atom (see Table SI in the supplementary material). Thus, although sizes of substituting atoms do affect local relaxation of the ions, it is also important to analyze the chemical bonds of the elements to explain the effect on the formation of ASP.

Furthermore, we have found that two ASPs $2(Cu_X^- + X_{Cu}^+)$ show also similar trends in the defect formation energy as a single ASP. In Cu_2MgSnS_4, Cu_2MnSnS_4, and Cu_2NiSnS_4, the defect formation energy of two complexes (i.e., $2(Cu_X^- + X_{Cu}^+)$) is a little smaller than the sum of the effects due to the presence of two single complexes. Therefore, ASP clusters and/or Cu–X disorder in are expected to be as strong as for Cu–Zn disorder in CZTS. For these compounds, the effect on the electronic structure depends on the concentration of the ASPs. For example, the shift in the gap energies for one ASP ($Cu_X^- + X_{Cu}^+$) is about $\Delta E_g \approx -0.1$ to -0.2 eV for Cu_2MgSnS_4, Cu_2MnSnS_4, Cu_2FeSnS_4, and CZTS; one ASP defect implies here 12.5% disorder. The corresponding energy shift of two ASPs (25% disorder; not presented in the table) is $\Delta E_g \approx -0.2$ to -0.4 eV for these four compounds. Since ($Cu_X^- + X_{Cu}^+$) narrows the gap and clustering enhances this effect, non-uniform distributions or concentrations of Cu–X disorder may imply spatial fluctuations of the band-gap energy in the material. However, the band-gap energy can be stabilized for forming, in addition to clusters of ($Cu_X^- + X_{Cu}^+$), clusters involving Cu-poor ($V_{Cu}^- + X_{Cu}^+$) defects that increase the gap energy. Here, clustering of neutral ($Cu_X^- + X_{Cu}^+$) with neutral ($V_{Cu}^- + X_{Cu}^+$) can occur due to relaxation effects and preferred octet formation, as modeled by Huang and Persson.[41] For Cu_2BeSnS_4 and Cu_2CaSnS_4, on the other hand, the corresponding energy shift due to two ASPs ($\Delta E_g \approx -0.4$ eV) is similar to the shift due to a sole ASP ($\Delta E_g \approx -0.3$ eV). This may indicate somewhat more localized charge distribution for ASP in these compounds, which is also supported by the stronger relaxation and larger shift ΔE_g for these compounds. The smaller additive effect is advantageous regarding disorder and may compensate for the larger shift for the low concentration of ASP.

The defect physics of Cu_2FeSnS_4 and Cu_2NiSnS_4 are somewhat different from that of the compounds discussed above and requires therefore a special discussion. For Cu_2FeSnS_4, the ASPs and Cu-poor ($V_{Cu}^- + X_{Cu}^+$) defects behave similar to Cu_2MnSnS_4, and being neutral, change the band gap energy moderately. However, the point defect Fe_{Cu} forms a localized defect level in the middle of the band gap region (see Fig. S2 in the supplementary material). If the point defect is uncompensated, for Fe-rich materials, it can be devastating for device performance. The Fe_{Cu} defects need thus to be avoided or to be fully compensated by for instance V_{Cu}^-. Moreover, both Fe_{Cu} and V_{Fe} narrow the band gap considerably (Table II), and thus, neither Fe-rich nor Fe-

poor materials are preferable unless these point defects are compensated.

Cu_2NiSnS_4 has very good optical properties due to energetically low-lying Ni d-like states at the CBM, which form flat CB. This compound does not have the same problem with point defects as Cu_2FeSnS_4; instead these defects are in much sense similar to the other CXTS. However, a striking difference is that Ni_{Cu} does not form shallow donor states. Instead, we find that Ni_{Cu} forms a magnetic defect and that E_F is inside the gap region of the host Cu_2NiSnS_4 (Fig. 4). Since Ni_{Cu} is not a shallow donor, the binding energies of the complexes $(V_{Cu} + Ni_{Cu})$ and $(Cu_{Ni} + Ni_{Cu})$ are small: $|E_b(D)| < 0.8$ eV. However, the defect formation energies of V_{Cu} and ASP $(Cu_{Ni} + Ni_{Cu})$ are as small as those for CZTS. Thus, the point defects can be less affected by compensation and thereby more mobile compared to the other compounds. Nevertheless, it will be difficult to avoid disorder from the high concentration of ASP also in Cu_2NiSnS_4. Moreover, the ASP forms more localized and magnetic defect states in the gap region. This can be devastating for a PV material, and thus, Cu_2NiSnS_4 is perhaps challenging to be utilized as a PV absorber.

IV. CONCLUSION

To conclude, employing the HSE06 method, we study the electronic and optical properties of CXTS (X = Be, Mg, Ca, Mn, Fe, and Ni) as well as the impact of their native defect pairs. First, the most stable ground-state phases of CXTS are estimated from the calculated total energies of different crystalline and magnetic configurations. We find that Cu_2MgSnS_4, Cu_2MnSnS_4, and Cu_2FeSnS_4 are stable in the ST phase D_{2d}^{11}, while Cu_2BeSnS_4 and Cu_2NiSnS_4 compounds favor the KS phase S_4^2 just like CZTS. The total energy difference to the second stable phase is however moderate, at most $\sim$0.25 eV per formula unit. The formation energies of CXTS (X = Be, Mg, and Ni) are similar to those of CZTS. However, Cu_2MnSnS_4 and Cu_2FeSnS_4 are clearly stable phases. Thereby, these compounds probably are more stable with high temperature or pressure during synthesis. Considering tetragonal phases, ST Cu_2CaSnS_4 has lower formation energy compared to its KS phase, but this compound prefers (just like Cu_2BaSnS_4) the trigonal C_3^2 crystalline structure. However, even with this phase, Cu_2CaSnS_4 is not stable with respect to decomposition.

Second, the considered CXTS compounds have suitable band-gap energies ($E_g = 1.2$–1.9 eV) for photovoltaic applications; here, Se-S alloying is expected to yield up to 0.5 eV smaller E_g, and thus, alloying can be applied for compounds with too large gap. Also, the absorption coefficients are very good: $\alpha(\omega) \approx (10$–$40) \times 10^4$ cm^{-1} at $E_g + 1.0$ eV. Here, Cu_2NiSnS_4 presents the best absorption for low-energy photons. However, for Cu_2NiSnS_4, the ASP yields localized defect states, and this compound may therefore not be suitable for PV applications. In addition, Ni_{Cu} does not act as a single donor like corresponding X_{Cu} in the other compounds.

Third, in all compounds (here, considering the trigonal structure of Cu_2CaSnS_4), a significant band-gap narrowing occurs in the presence of Cu_X or X_{Cu} and consequently also with their defect pair $(Cu_X + X_{Cu})$. For the anti-site pair, the shift is $\Delta E_g \approx -0.1$ to -0.2 eV with 12.5% disorder concentration for Cu_2MgSnS_4, Cu_2MnSnS_4, Cu_2FeSnS_4, and Cu_2ZnSnS_4, whereas it is twice as a large impact ($\Delta E_g \approx -0.2$ to -0.4 eV) for Cu_2BeSnS_4 and trigonal Cu_2CaSnS_4. As expected from the Cu-d–S-p repulsion of the VB states, the gap energies are increased by the presence of not only V_{Cu} but also $(V_{Cu} + X_{Cu})$, which indicates that V_{Cu} rules over X_{Cu}; the exception is for Cu_2FeSnS_4 and Cu_2NiSnS_4 with less trivial X_{Cu} defects.

Fourth, due to the low formation energy of $(Cu_X + X_{Cu})$, we conclude that it is difficult to avoid disordering from the high concentration of these ASPs in most of the CXTS compounds. However, in Cu_2BeSnS_4, the formation energy is higher, and we expect $\sim$10^4 times lower concentration of the disordering at room and operating temperatures than for the other compounds. We compare the trigonal Ca-compound with the other tetragonal compounds because there can be structural effects. Moreover, the Ca-compound is not stable. Our focus is on tetragonal structures. The lower concentration in Cu_2BeSnS_4 is explained partly by the larger relaxation effects in these two compounds as the difference between Cu and the two anti-site atoms of Be is more obvious than those between Mg, Mn, Fe, or Zn. However, relaxation effects due to sizes of cations cannot fully describe the formation energies of substitutes, and the properties of the chemical elements are also important to be considered. The disadvantage of ASP with different atom sizes is that the stronger relaxation influences the electronic structure, and the band-gap narrowing $|\Delta E_g|$ is larger for a given defect concentration for Cu_2BeSnS_4. Moreover, Be is a toxic element and difficult to handle in synthesis processes, which makes it less favorable. Cu_2CaSnS_4, on the other hand, is not stable in the tetragonal phase nor in its trigonal phase. The stability of Cu_2MgSnS_4 is contradictorily predicted using DFT.[17,18] One may speculate the impact of ASP for other CXTS compounds and also related chalcopyrite materials, but further studies and development of the compounds and their native point defects and ASP are required. Moreover, we expect that corresponding Se-based compounds Cu_2XSnSe_4 are expected to have similar defect properties as the S-based compounds Cu_2XSnS_4, and also, this has to be investigated.

SUPPLEMENTARY MATERIAL

See supplementary material for the complementary band structure and DOS of Cu_2FeSnS_4 in Fig. S1, the total DOS of compounds with defects V_{Cu}, Cu_X, X_{Cu}, and $(Cu_X + X_{Cu})$, as well as the corresponding DOS for the defect free case: (a) Cu_2MgSnS_4, (b) Cu_2CaSnS_4, (c) Cu_2FeSnS_4, and (d) Cu_2ZnSnS_4 in Fig. S2, and complementary defect energies of the trigonal phase of Cu_2CaSnS_4 and the tetragonal ST phases of Cu_2CdSnS_4 in Table SI.

ACKNOWLEDGMENTS

[1]W. Wang, M. T. Winkler, O. Gunawan, T. Gokmen, T. K. Todorov, Y. Zhu, and D. B. Mitzi, Adv. Energy Mater. **4**, 1301465 (2014).

[2]*Copper Zinc Tin Sulphide-Based Thin Film Solar Cells*, edited by K. Ito (John Wiley & Sons, Chichester, 2015).

[3]S. Schorr, Sol. Energy Mater. Sol. Cells **95**, 1482 (2011).

[4]J. J. S. Scragg, J. K. Larsen, M. Kumar, C. Persson, J. Sendler, S. Siebentritt, and C. Platzer-Björkman, Phys. Status Solidi B **253**, 247 (2016).

[5]S. Chen, J.-H. Yang, X. G. Gong, A. Walsh, and S.-H. Wei, Phys. Rev. B **81**, 245204 (2010).

[6]A. Nagoya, R. Asahi, R. Wahl, and G. Kresse, Phys. Rev. B **81**, 113202 (2010).

[7]S. Siebentritt and S. Schorr, Prog. Photovoltaics **20**, 512 (2012).

[8]M. Kumar, H. Zhao, and C. Persson, Thin Solid Films **535**, 318 (2013).

[9]S. Bourdais, C. Chon, B. Delatouche, A. Jacob, G. Larramona, C. Moisan, A. Lafond, F. Donatini, G. Rey, S. Siebentritt, A. Walsh, and G. Dennler, Adv. Energy Mater. **6**, 1502276 (2016).

[10]L. Chen, H. Deng, J. Tao, H. Cao, L. Huang, L. Sun, P. Yang, and J. Chu, RSC Adv. **5**, 84295 (2015).

[11]L. Li, X. Liu, J. Huang, M. Cao, S. Chen, Y. Shen, and L. Wang, Mater. Chem. Phys. **133**, 688 (2012).

[12]X. Zhang, N. Bao, K. Ramasamy, Y. H. A. Wang, Y. Wang, B. Lin, and A. Gupta, Chem. Commun. **48**, 4956 (2012).

[13]B. Murali, M. Madhuri, and S. B. Krupanidhi, Cryst. Growth Des. **14**, 3685 (2014).

[14]T.-X. Wang, Y.-G. Li, H.-R. Liu, H. Li, and S.-X. Chen, Mater. Lett. **124**, 148 (2014).

[15]A. Kamble, K. Mokurala, A. Gupta, S. Mallick, and P. Bhargava, Mater. Lett. **137**, 440 (2014).

[16]M. Wei, Q. Du, R. Wang, G. Jiang, W. Liu, and C. Zhu, Chem. Lett. **43**, 1149 (2014).

[17]C. Wang, S. Chen, J. H. Yang, L. Lang, H. J. Xiang, X. G. Gong, A. Walsh, and S.-H. Wei, Chem. Mater. **26**, 3411 (2014).

[18]G. Zhong, K. Tse, Y. Zhang, X. Li, L. Huang, C. Yang, J. Zhu, Z. Zeng, Z. Zhang, and X. Xiao, Thin Solid Films **603**, 224 (2016).

[19]B. G. Mendis, M. D. Shannon, M. C. J. Goodman, J. D. Major, A. A. Taylor, D. P. Halliday, and K. Durose, J. Phys. Conf. Ser. **471**, 012014 (2013).

[20]Z.-K. Yuan, S. Chen, H. Xiang, X.-G. Gong, A. Walsh, J.-S. Park, I. Repins, and S.-H. Wei, Adv. Funct. Mater. **25**, 6733 (2015).

[21]A. Crovetto, R. Chen, R. B. Ettlinger, A. C. Cazzaniga, J. Schou, C. Persson, and O. Hansen, Sol. Energy Mater. Sol. Cells **154**, 121 (2016).

[22]C. H. Henry, J. Appl. Phys. **51**, 4494 (1980).

[23]W. Shockley and H. J. Queisser, J. Appl. Phys. **32**, 510 (1961).

[24]G. Kresse and D. Joubert, Phys. Rev. B **59**, 1758 (1999).

[25]G. Kresse and J. Furthmüller, Phys. Rev. B **54**, 11169 (1996).

[26]J. P. Perdew, K. Burke, and M. Ernzerhof, Phys. Rev. Lett. **77**, 3865 (1996).

[27]J. P. Perdew, A. Ruzsinszky, G. I. Csonka, O. A. Vydrov, G. E. Scuseria, L. A. Constantin, X. Zhou, and K. Burke, Phys. Rev. Lett. **100**, 136406 (2008).

[28]V. I. Anisimov, J. Zaanen, and O. K. Andersen, Phys. Rev. B **44**, 943 (1991).

[29]C. E. Cava, L. S. Roman, and C. Persson, Phys. Rev. B **88**, 045136 (2013).

[30]W. Setyawan, R. M. Gaume, S. Lam, R. S. Feigelson, and S. Curtarolo, ACS Comb. Sci. **13**, 382 (2011).

[31]C. Persson, C. Dong, L. Vayssieres, A. Augustsson, T. Schmitt, M. Mattesini, R. Ahuja, J. Nordgren, C. Chang, A. Ferreira da Silva, and J.-H. Guo, Microelectron. J. **37**, 686 (2006).

[32]J. Heyd, G. E. Scuseria, and M. Ernzerhof, J. Chem. Phys. **118**, 8207 (2003).

[33]D. Shin, B. Saparov, T. Zhu, W. P. Huhn, V. Blum, and D. B. Mitzi, Chem. Mater. **28**, 4771 (2016).

[34]T. Fries, Y. Shapira, F. Palacio, M. C. Morón, G. J. McIntyre, R. Kershaw, A. Wold, and E. J. McNiff, Phys. Rev. B **56**, 5424 (1997).

[35]P. Bonazzi, L. Bindi, G. P. Bernardini, and S. Menchetti, Can. Miner. **41**, 639 (2003).

[36]S. Schorr, H. J. Hoebler, and M. Tovar, Eur. J. Miner. **19**, 65 (2007).

[37]S. R. Hall, J. T. Szymanski, and J. M. Stewart, Can. Mineral. **16**, 131 (1978).

[38]P. M. P. Salomé, J. Malaquias, P. A. Fernandes, M. S. Ferreira, A. F. da Cunha, J. P. Leitão, J. C. González, and F. M. Matinaga, Sol. Energy Mater. Sol. Cells **101**, 147 (2012).

[39]H. Zhao and C. Persson, Thin Solid Films **519**, 7508 (2011).

[40]C. Persson, S. Lany, Y.-J. Zhao, and A. Zunger, Phys. Rev. B **72**, 035211 (2005).

[41]D. Huang and C. Persson, Thin Solid Films **535**, 265 (2013).